Dimensional Analysis of Absorbency in Paper Towels: A Study of Three- and Two-Dimensional Mechanisms

Soon Wan Kweon, Na Young Kang, and Hyoung Jin Kim *

The dimensional absorbency properties of paper towels were studied, focusing on three- and two-dimensional absorption mechanisms. Key factors affecting these absorption mechanisms were identified through a series of experiments and principal component analysis (PCA). The results showed that the water absorption capacity, driven by capillary action (porosity), exhibited differences between two-dimensional surface absorption (in the X and Y directions) and three-dimensional bulk absorption (including the Z direction, or thickness). Porosity analysis revealed that three-dimensional absorbency is highly correlated with porosity, whereas two-dimensional absorbency has a relatively low correlation and is influenced by fiber properties such as length and width, as well as mass-related characteristics including fines content and freeness. The findings highlight the need to balance these dimensional properties to achieve optimal absorbency in paper towel products. Additionally, this study provides a foundation for developing more efficient paper towels and offers valuable insights into the complex mechanisms of paper towel absorbency, which will aid in the development of improved hygiene paper products.

DOI: 10.15376/biores.20.1.683-697

Keywords: Paper towel; Absorbency; Dimensional; Principal component analysis (PCA); Surface properties; RMAD; FMAD; Image analysis; PicMan

Contact information: Department of Forest Products and Biotechnology, Kookmin University, 77 Jeongneung-ro, Seongbuk-gu, Seoul 02707 Republic of Korea;
** Corresponding author: hyjikim@kookmin.ac.kr*

INTRODUCTION

Disposable hygiene products are essential consumer goods in modern life, playing a significant role in maintaining hygiene and cleanliness across various environments, from homes to industrial settings. The global market for tissue products is expanding annually, driven by advantages such as low cost, availability of raw materials, ease of disposal, and efficient manufacturing processes, ensuring continued growth (Hansen *et al*. 2013). Disposable hygiene products can be classified into two groups: hygiene paper and disposable absorbents (Ko *et al*. 2016). The first group includes toilet tissues, facial tissues, paper towels, and napkins, while the second group encompasses baby diapers, sanitary napkins, and incontinence pads.

Sanitary paper products require softness, strength, and absorbency, with each product developed to emphasize different characteristics based on user needs. This is also influenced by fiber type, with chemical pulp and virgin fibers generally offering excellent strength and softness, while recycled fibers tend to produce products with relatively lower strength and reduced softness (de Assis *et al*. 2018).

For paper towels, absorbency—the ability to hold and absorb liquid—is a particularly crucial characteristic as it directly affects the performance and usability of the paper towel in various applications (Ko *et al*. 2017). These properties are controlled and tailored through the manufacturing process of the fibers, which creates the porous and fibrous structure of paper towels (Hodgson and Berg 2007; Brodin and Theliander

2012). The primary ability to absorb and retain liquids makes paper towels indispensable for tasks such as wiping up spills, drying hands, and cleaning surfaces. Absorbency is influenced by several factors, including fiber composition, multilayer ply structure, and surface properties. Given the widespread use and importance of paper towels, understanding their absorption mechanisms and influencing factors, and developing products that utilize this understanding, is essential to improving their performance and efficiency.

A key consideration in absorbency performance is the balance between absorbency rate (how quickly liquid is absorbed) and absorbency capacity (the total amount of liquid the towel can hold). These two properties often need to be balanced carefully, as focusing solely on a high absorbency rate may reduce the total capacity of the towel, while maximizing capacity might slow down the absorption rate. Multilayered structures provide a solution to this trade-off. This approach ensures that the product can quickly absorb spills while holding a significant amount of liquid, thereby optimizing performance in real-world applications.

Capillary action, or capillarity, is considered the key mechanism and basic theory that governs the absorbency of paper towels (Beuther *et al*. 2010). The driving force that moves liquid from the surface into the interior of the paper is capillary pressure, which is the differential pressure across the curved meniscus of the liquid-air interface in a capillary (Ko *et al*. 2016). This refers to the ability of a liquid to flow through a narrow space without external forces, even against gravity. While classical capillary theory often assumes cylindrical shapes for capillaries, in the fiber network of paper towels, the capillaries are highly irregular. The fibers form random, non-uniform pores and channels, leading to capillaries that are not perfect cylinders but rather vary in size and shape. This irregularity affects the movement of liquid by creating variable capillary pressures throughout the structure. Some regions may facilitate faster liquid flow due to larger, more open capillaries, while others with narrower, irregular spaces may slow the liquid's movement. This non-cylindrical capillary network contributes to the overall absorbency by promoting both surface spreading and deeper penetration into the paper's structure, creating a more dynamic and efficient absorption process. Ko (1981) described this complex structure through three cases of pressure gradients, termed capillary flow/pumps, which reflect irregularities found in paper towel fiber networks. This principle involves spreading the liquid across the surface and penetrating the deeper layers of the paper towel, providing a three-dimensional absorbent basis.

The moisture absorption mechanism of paper towels consists of two steps. The first step involves moisture absorption from the surface, while the second step entails the movement of moisture from the surface into internal pores (or capillaries). The moisture absorption mechanism in the first step can be described as a two-dimensional absorption mechanism, focusing on the lateral diffusion of the liquid across the plane of the paper towel. Additionally, the overall absorption mechanism encompassing both phases can be described as a three-dimensional absorption mechanism involving both lateral (*i.e.*, X- or Y-direction) diffusion and Z-direction (*i.e.*, thickness direction) penetration. Absorptivity can thus be analyzed in both two-dimensional and three-dimensional contexts. Understanding these mechanisms is important for improving the design and functionality of paper towels.

While many studies have examined the individual roles of fiber composition, porosity, bulk, and density in the absorbency of paper products, limited research has focused on the correlation between these properties and how they collectively influence absorbency. Existing literature, such as Brodin and Theliander (2012) and Beuther *et al*. (2010), suggests that absorbency is a multifactorial property, where factors such as fiber morphology and porosity interact to impact liquid uptake. However, there is a gap

in understanding how these factors influence absorbency in a dimensional context, particularly when comparing 2D and 3D mechanisms. This study aimed to address this gap by incorporating a broader analysis of existing research to contextualize the findings and to highlight how fiber properties, porosity, density, and surface characteristics interact to affect overall performance.

Therefore, this study provides a comprehensive understanding of moisture absorption behavior (two- and three-dimensional) by dimensionally classifying the absorption mechanism, which is a primary characteristic of paper towels, and identifying influencing factors. Three-dimensional water absorption analysis was performed according to ISO 12625-8 (2022). In addition, to analyze the two-dimensional absorption mechanism, a custom device was developed to inject a fixed amount of liquid, and advanced imaging techniques were utilized to analyze the wetting behavior. This series of processes aimed to characterize the absorption mechanism through principal component analysis (PCA).

EXPERIMENTAL

Paper Towel Samples

The physical properties of seven paper towel samples, obtained from various commercial sources (sample codes: A, B, C, D, E, F, G), were tested. Table 1 lists these samples along with some key physical attributes. All samples were 2-ply products, created by laminating two plies together.

Optical photographs of the samples were captured using the Optitopo Surface Deviation (OSD, L&W, Sweden) apparatus. Given that all products consisted of two plies, no discernible pattern variation was observed between the top and bottom layers in the optical images. Figure 1 shows the top layers of the seven paper towel samples, with arrows indicating the machine direction (MD).

Table 1. Physical Properties of the Commercial Paper Towel Samples

Sample code	Basis weight (g/m^2)	Thickness (mm)	Density (g/cm^3)	Country	Dry technology*	Type
A	53.7	0.29	0.19	USA	TAD	All-virgin, embossed
B	52.2	0.30	0.17	USA	TAD	
C	41.1	0.15	0.27	Korea	DCT	
D	37.4	0.16	0.24	Korea	DCT	
E	43.2	0.18	0.24	Korea	DCT	
F	40.3	0.15	0.27	Korea	DCT	
G	40.0	0.16	0.24	Korea	DCT	

Note) number of plies in all sample: 2
**TAD: Through-Air Drying; DCT: Dry Crepe Technology*

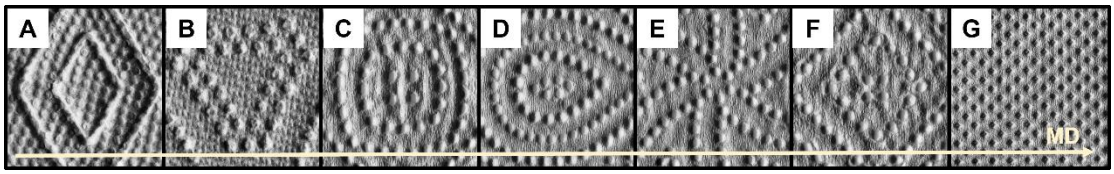

Fig. 1. Optical photographs of the commercial paper towel samples

Fiber Analysis of Paper Towels

The properties of paper towel fibers were analyzed through a series of standardized tests. Disintegration was conducted according to ISO 5263-1, with a pH 10 condition using sodium hydroxide (NaOH, Deajung, Korea, 97%) to counteract the impact of wet strength resin treatment on disintegration efficiency. The average fiber length and width for each sample were measured using a Fiber Tester (Fiber Tester Plus, Lorentzen & Wettre, Sweden) in accordance with ISO 16065-2. This involved using 0.1 g of fiber in 200 mL of water. Additionally, the freeness of each fiber, which indicates the dewatering potential of the pulp suspension on the pulp and paper machine's wire, was assessed following ISO 5267-2 standards. Each sample was measured 10 times to ensure accuracy. Porosity, a critical factor in absorbency due to capillary action, was calculated using Eq. 1 (Henriksson *et al.* 2008; Tanpichai *et al.* 2012; Tanpichai *et al*. 2019),

$$Porosity\ (\%) = \left[1 - \left(\frac{density\ of\ paper\ towel\ sample}{density\ of\ cellulose}\right)\right] X\ 100 \quad (1)$$

where the density of cellulose is 1.5 g/cm^{-3}.

Surface Properties Analysis of Paper Towels

To analyze the surface characteristics of the paper towels, a direct measurement method was employed using a surface tester (KES-SESRU, Kato Tech Co., Ltd., Kyoto, Japan) to extract surface roughness (*R*) and surface friction (*F*) profiles (Park 2017; Ko *et al*. 2018; Moon 2021; Lee *et al*. 2023; Kweon *et al*. 2024). A U-tube type probe was used for profile extraction under the measurement conditions specified in ISO 12625-18 (2022): contact force of 5 gf, scan length of 20 mm, and scan speed of 1.0 mm/s. The commercial KES surface tester has a resolution of 10 Hz, corresponding to a sampling distance of 100 μm. To enhance the sampling distance to 10 μm, a data logger (Midi Logger GL900, Graptec, Japan) was used with a data acquisition rate set to 100 Hz. The relationship between data acquisition rate and sampling distance has been detailed in previous research (Park *et al*. 2021).

For each sample, 10 replicate measurements were conducted in the machine direction (MD) and cross-machine direction (CD), and the average of the extracted profiles was used. The configuration and setup of the measuring equipment are shown in Fig. 2. The extracted surface profile data were analyzed using the formulas in Table 2. This analysis involved calculating the average roughness (R_a) and the mean absolute deviation from R_a (*RMAD*), as well as the average coefficient of friction ($\bar{\mu}$) and its mean absolute deviation (*FMAD*). Additionally, each profile data was analyzed for variability by calculating the coefficient of variation (COV), a statistical indicator that measures the relative variability of the data set. COV is calculated by dividing the standard deviation by the mean, then multiplying by 100 to express it as a percentage. A higher COV indicates greater variability relative to the mean, while a lower COV suggests more consistency. This metric allows for comparison of variability across datasets with different units or scales, making it useful for analyzing the relative variation among samples.

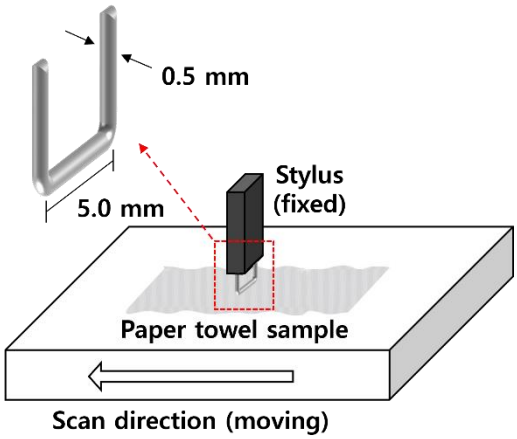

Fig. 2. Configuration of the surface tester and geometry of single-wire-type stylus

Table 2. Surface Roughness and Friction Calculation Formula

Surface Roughness	Surface Friction
$R_i = h_i - \bar{h}$ $R_a = \frac{1}{N}\sum_1^N R_i$ $RMAD = \frac{1}{N}\sum_1^N \lvert R_i - R_a \rvert$	COF = drag force / contact force $\bar{\mu} = \frac{1}{N}\sum_1^N \mu_i$ $FMAD = \frac{1}{N}\sum_1^N \lvert \mu_i - \bar{\mu} \rvert$
h_i: the height at a scanning point *i* $\bar{h}$: the average of height N: the number of data points in the scan length R_i: the roughness (µm) at a scanning point *i* R_a: the roughness average (µm)	N: the number of data points from the scan length μ_i: the COF at a scanning point *i* $\bar{\mu}$: the average COF, MIU

Figure 3(a) provides a graphical representation of R_i, R_a and *RMAD*, where *RMAD* is calculated by dividing the shaded area by the scan length and is shown as a dotted line. In calculating *RMAD*, R_a is treated as a constant, similar to how thickness average is treated as a constant in calculating R_a. Figure 3(b) shows the friction profile of the friction coefficient versus scan length. *FMAD* is calculated by dividing the shaded area by the scan length and is shown as a dashed line. When calculating *FMAD*, $\bar{\mu}$ is treated as a constant, similar to the calculation of *RMAD*.

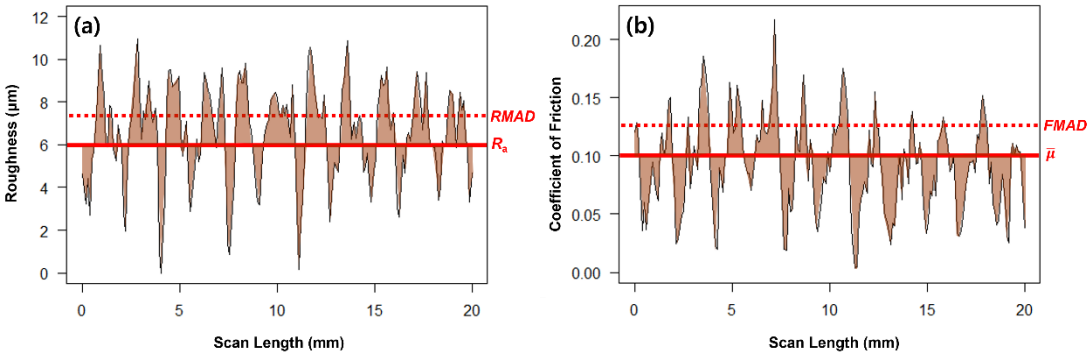

Fig. 3. Graphical representation (a: R_i, R_a, and *RMAD*; b: μ_i, $\bar{\mu}$ (MIU) and *FMAD*)

Three-Dimensional Absorption Testing

To measure the three-dimensional absorption capacity of the paper towel samples, a basket immersion test was conducted in accordance with ISO 12625-8. This method involves immersing the samples in water and measuring the mass of water absorbed per unit mass of the test specimen. The moisture absorption measured through this method includes simultaneous absorption in both the plane and Z-direction (*i.e.*, thickness direction), representing a comprehensive three-dimensional wicking process.

Two-Dimensional Absorption Testing

The two-dimensional absorbency mechanism of the paper towels was examined using an optical microscope, referring to the study of Abedsoltan (2022). Images were captured with a USB digital microscope to document the sample surfaces. Wetted area analysis was performed using the Free Form function of the image processing and analysis software PicMan (WaferMasters, Inc., Dublin, CA, USA). For the two-dimensional absorption analysis, all samples were separated into layers, and only the top layer was analyzed. To ensure consistent water droplet deposition, a syringe pump (Legato® 100, kdScientific, Korea) was used. 5 mL of water was put into a 20 mL syringe and injected at a flow rate of 0.2 mL/min. An 18G needle (inner diameter: 1.2 mm) was used, maintaining a fixed distance of 150 mm between the needle tip and the sample surface for the two-dimensional absorption performance test. Each drop delivered from the syringe and needle setup represented approximately 0.05 mL of water, ensuring precise control over both flow rate and drop size. This consistency in water delivery allowed for uniform application to each sample. Absorbency measured by this method occurs due to radial water absorption, which can be considered two-dimensional radial wicking, ignoring the Z-direction. Figure 4 presents a schematic diagram of the two-dimensional wetting process.

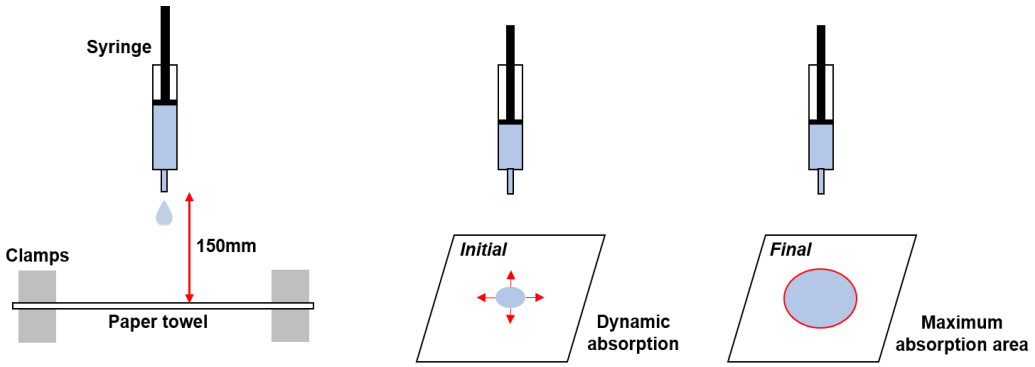

Fig. 4. Schematic of the two-dimensional wetting process

Principal Component Analysis (PCA)

Principal component analysis (PCA) is a dimensionality reduction technique that transforms many correlated variables into a smaller number of uncorrelated variables. It is widely used for analyzing and visualizing characteristics in classification and identification fields. Figure 5 provides a conceptual visualization of PCA.

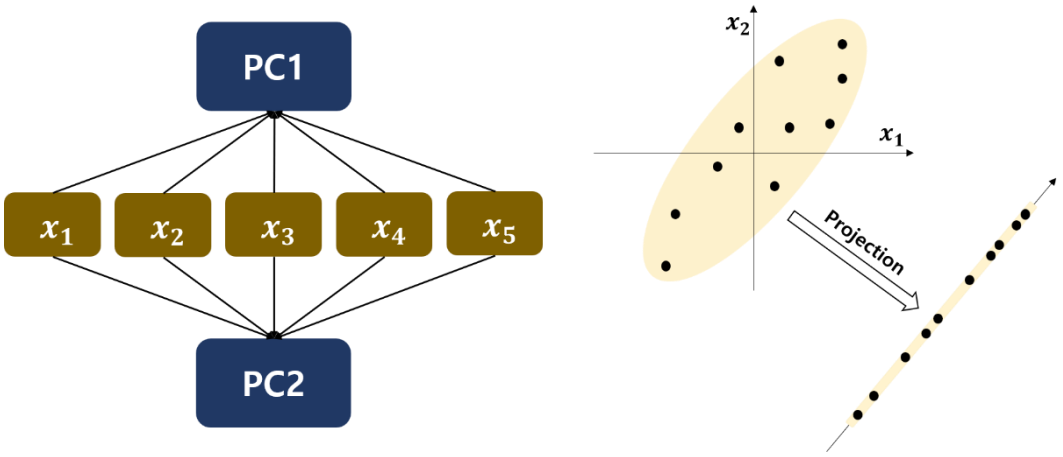

Fig. 5. Conceptual example of principal component analysis (Kweon *et al*. 2023).

In this study, PCA was performed using R software (R Core Team, ver. 4.3.0, Auckland, New Zealand) to analyze the primary factors affecting the dimensional absorption mechanism of paper towels. The analysis was based on 10 repeated measurements of porosity, density, *RMAD*, *FMAD*, freeness, fiber length, fiber width, and fines data for each sample. Each dataset was preprocessed through normalization, converting variable values to a range between 0 and 1 using Eq. 2. In this equation, $X_n = 1$ when $X = X_{max}$ and $X_n = 0$ when $X = X_{min}$.

$$X_n = (X - X_{min})/(X_{max} - X_{min}) \quad (2)$$

where X_n is the normalized value of X, X_{min} is the minimum value of X, and X_{max} is the maximum value of X.

Following normalization, the covariance matrix was calculated, and the eigenvalues and eigenvectors were extracted to visualize and evaluate the impact of each feature on the dimensional absorption mechanism.

RESULTS AND DISCUSSION

Fiber Analysis Results

Table 3 presents the average fiber length, average fiber width, fines content, and freeness of the paper towel samples used in this study. Fiber length analysis revealed that samples A and B had relatively long fibers compared to the rest of the samples. Sample B exhibited the widest fiber width, while the other samples had similar fiber widths. The distribution of fines varied among the samples. Freeness values ranged from 670 to 740 mL CSF.

The difference values for both average fiber length and average fiber width, included in Table 3, represent the deviation of individual measurements from the average and provide insights into the variability across the samples. Based on these values, the analysis indicates that the variability of the measurements was low.

Table 3. Fiber Analysis Results of the Seven Paper Towel Samples

Code	Average Fiber Length (mm)	Average Fiber Width (μm)	Fines (%)	Freeness (mL CSF)
A	1.43 ± 0.094	21.8 ± 0.7	11.2	700
B	1.74 ± 0.003	28.0 ± 0.6	21.0	670
C	0.89 ± 0.064	19.0 ± 0.2	11.0	700
D	0.83 ± 0.016	18.9 ± 0.2	9.6	740
E	1.01 ± 0.008	19.0 ± 0.1	15.1	690
F	0.93 ± 0.023	19.7 ± 0.2	8.7	710
G	0.88 ± 0.041	21.2 ± 0.7	15.4	720

Surface Properties Analysis Results

Tables 4 and 5 summarize the surface properties of the seven paper towel samples. R_a, *RMAD*, $\bar{\mu}$, and *FMAD* were calculated as per the formulas in Table 2. The geometric mean (GM) was determined as the square root of the product of the MD and CD values.

Table 4. Surface Roughness Properties of the Seven Commercial Paper Towel Samples

Code	R_a						*RMAD*					
	Mean (μm)			COV (%)			Mean (μm)			COV (%)		
	MD	CD	GM	MD	CD	GM	MD	CD	GM	MD	CD	GM
A	5.45	4.33	4.96	14.5	37.8	23.4	1.42	1.16	1.28	13.7	22.5	17.6
B	5.52	5.30	5.48	18.9	23.1	20.9	1.48	1.35	1.42	10.1	15.9	12.7
C	9.78	6.58	8.10	17.7	24.6	20.9	2.07	1.61	1.82	11.3	17.1	13.9
D	6.19	4.19	5.11	14.7	17.6	16.1	1.80	1.31	1.53	10.3	15.8	12.8
E	9.43	6.04	7.34	33.4	25.8	29.4	1.93	1.46	1.68	12.1	18.0	14.8
F	11.56	7.90	9.57	18.6	23.6	21.0	2.31	1.67	1.96	13.4	14.8	14.1
G	5.62	4.64	5.16	16.4	13.0	14.6	1.74	1.24	1.47	10.5	11.0	10.8

Table 5. Surface Friction Properties of the Seven Commercial Paper Towel Samples

Code	$\bar{\mu}$						*FMAD*					
	Mean			COV (%)			Mean			COV (%)		
	MD	CD	GM	MD	CD	GM	MD	CD	GM	MD	CD	GM
A	0.38	0.34	0.36	26.8	33.4	29.9	0.13	0.11	0.12	20.0	19.2	19.6
B	0.33	0.26	0.29	15.3	32.6	22.3	0.10	0.10	0.10	15.9	27.7	21.0
C	0.47	0.39	0.43	24.0	25.4	24.7	0.16	0.11	0.13	7.3	21.3	12.5
D	0.45	0.28	0.35	23.9	34.5	28.7	0.15	0.08	0.11	18.7	26.4	22.2
E	0.36	0.36	0.36	27.5	29.4	28.4	0.13	0.12	0.13	26.9	27.6	27.3
F	0.47	0.50	0.48	26.2	31.5	28.7	0.16	0.14	0.15	18.2	32.2	24.2
G	0.31	0.31	0.31	19.4	18.6	19.0	0.10	0.07	0.08	18.4	14.8	16.5

Figure 6(a) shows the regression equation between *RMAD* and R_a, parameters of surface roughness, with an R^2 value of 0.90, indicating a very high correlation. The regression equation's slope was significantly smaller than 1, suggesting that *RMAD* is less sensitive to changes in R_a values. This can be attributed to R_a being influenced by equipment and operating conditions in stylus-type contact methods, whereas *RMAD* is more independent and reflects within-sample variations. Therefore, *RMAD* represents the absolute change in the surface roughness profile of the sample.

Figure 6(b) presents the regression equation between *FMAD* and $\bar{\mu}$, parameters of surface friction, with an R^2 value of 0.84, indicating a high correlation. The slope of the regression equation was 0.30, suggesting that *FMAD* was less sensitive to changes in the $\bar{\mu}$ value. While $\bar{\mu}$ is influenced by equipment and operating conditions in the stylus contact method, *FMAD* represents the deviation from $\bar{\mu}$ and is not dependent on test conditions. Therefore, *FMAD* can be interpreted as the absolute change in the sample friction profile, reflecting variations within the sample.

In addition, the coefficients of variation (COV) for *RMAD* and *FMAD* were lower than those for R_a and $\bar{\mu}$, respectively (Tables 4 and 5). This supports the argument that *RMAD* and *FMAD* are measures of the true surface profile, unlike R_a and $\bar{\mu}$, which vary depending on test conditions. This indicates that R_a and $\bar{\mu}$ are treated as constants in the calculations of *RMAD* and *FMAD*, respectively. These findings are consistent with previous studies on surface parameter analysis (Ko *et al*. 2019).

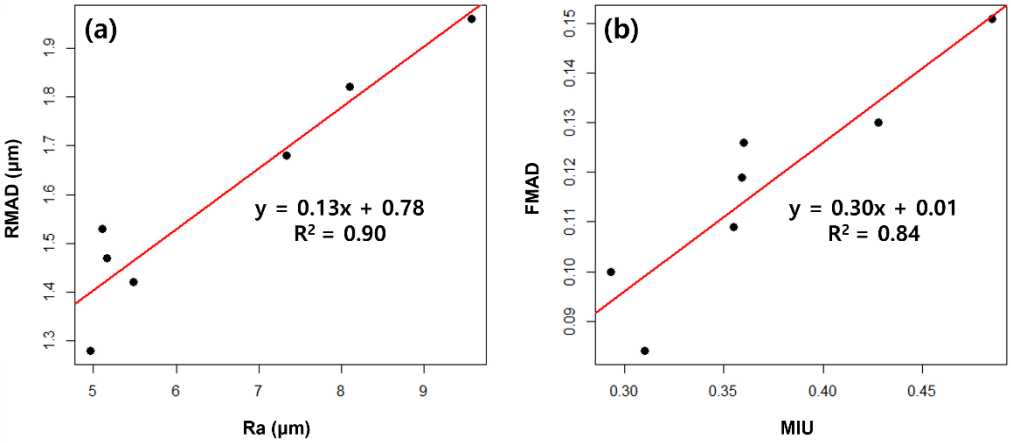

Fig. 6. Surface parameter analysis (a: *RMAD* vs. R_a; b: *FMAD* vs. $\bar{\mu}$)

In this study, surface characterization was conducted using *RMAD* and *FMAD* as the primary surface characterization parameters. *RMAD* was utilized as an indicator of surface roughness, with lower values indicating reduced surface roughness. Similarly, *FMAD*, representing the surface friction value, was used as an indicator of surface softness, where lower values denote less friction and thus a softer surface (Park *et al*. 2020; Kweon *et al*. 2024).

Three- and Two-Dimensional Absorption Results

The wetted area over time for two-dimensional water absorption was analyzed, and the results are presented in Fig. 7. For samples A and B, the initial absorption rate was high; however, it decreased over time compared to the other samples. In contrast, sample F exhibited a low initial absorption rate, indicating different absorption mechanisms among the samples. Furthermore, the maximum wetted area measured at 40 sec. showed significant differences between samples within the error range.

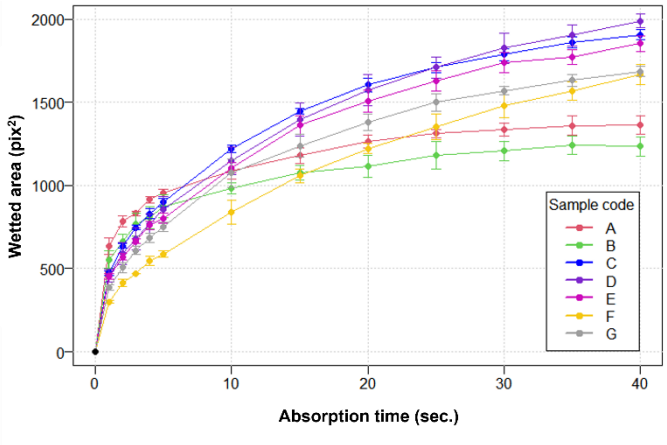

Fig. 7. Wetted area analysis results over time of the seven paper towel samples

Figure 8 shows the three- and two-dimensional absorbency measurement results. For three-dimensional absorbency, the maximum absorption capacity is indicated, whereas for two-dimensional absorbency, the maximum absorption area is shown. The analysis confirmed that the same sample exhibited different absorptive capacities depending on the dimension.

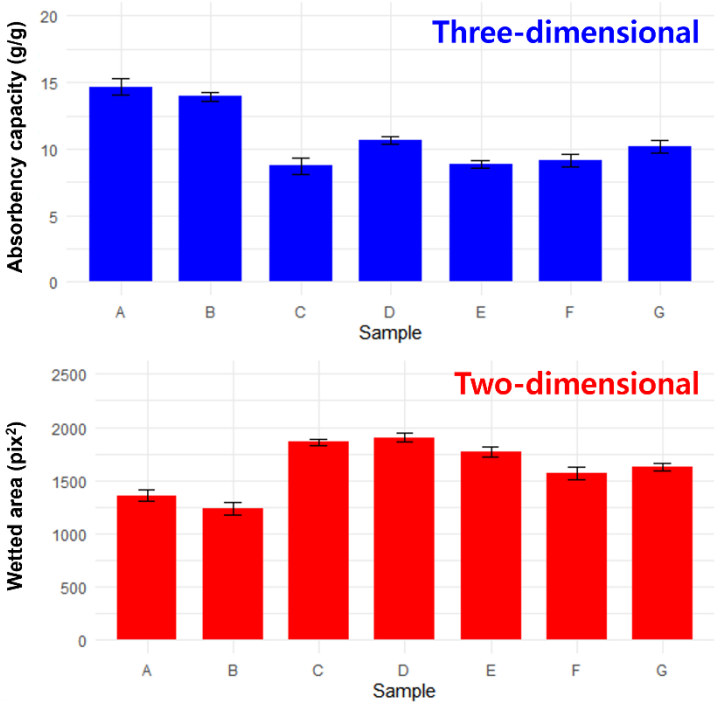

Fig. 8. Three- and two-dimensional absorbency analysis results of the seven paper towel samples

Analysis of Absorbency Capillary Action Along Dimensions

Figure 9 shows the regression analysis results for the correlation between porosity and water absorption rate according to dimension. Porosity plays a crucial role in the interaction of the sample surface with the liquid. Liquids penetrate the paper either through external pressure or internal forces that draw the liquid into the paper through a capillary system, implying penetration in the Z-direction. The analysis revealed that three-dimensional absorbency was directly proportional to porosity with a high correlation (R^2 = 0.86), while two-dimensional absorbency was inversely proportional to porosity with a relatively low correlation. Thus, for three-dimensional absorbency, capillarity due to porosity is the main absorption mechanism. However, for

two-dimensional absorbency, which occurs in the planar direction, other factors likely contribute to the absorption mechanism, necessitating further analysis.

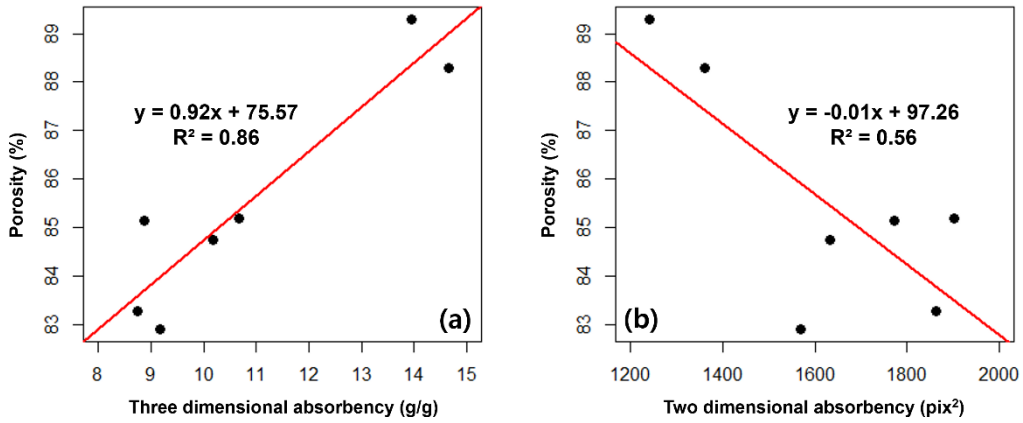

Fig. 9. Regression analysis of dimensional absorbency and porosity (a: three-dimensional absorbency; b: two-dimensional absorbency)

Principal Component Analysis (PCA)

Figure 10 shows the PCA analysis results of absorbency according to dimensions in a matrix diagram. The lower and left axes of the PCA matrix diagram represent the component scores of the first component (PC1) and the second component (PC2), respectively. This allows for the inference of relationships between variables or the correlation between components and variables.

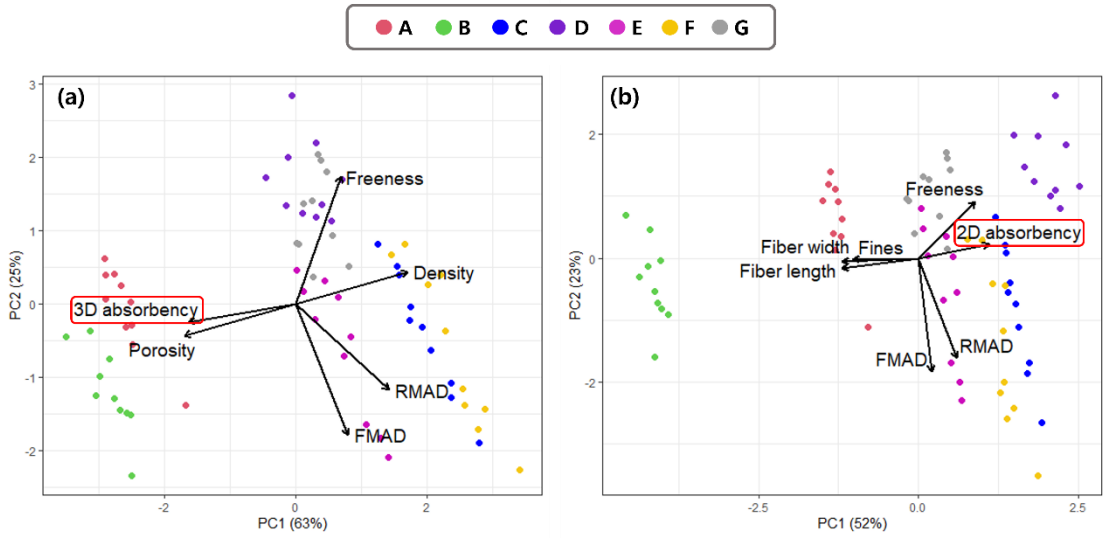

Fig. 10. Absorbency principal component analysis results (a: three-dimensional absorbency; b: two-dimensional absorbency)

The direction and angle of the vector on the PCA matrix diagram represent the relationships between variables. If the angle between the vectors is narrow and close to each other, the two variables represented by the vectors are interpreted as having a positive (+) correlation. In contrast, if the vectors meet at a right angle, the two variables are interpreted as not correlated. If the vectors form a wide angle and are spread in opposite directions, the two variables are interpreted as having a negative (−) correlation.

Figure 10(a) shows the PCA results for three-dimensional absorbency. The analysis found a positive correlation between porosity properties, and a negative correlation with density. Additionally, no correlation was found between fiber freeness and surface properties. Therefore, it is believed that three-dimensional absorbency is primarily influenced by porosity, indicating that capillary action in the Z-direction due to the multilayer structure is a major factor in the absorption mechanism.

In contrast, Fig. 10(b) shows the PCA results for two-dimensional absorbency. The analysis revealed that two-dimensional absorbency had a high correlation with fiber length, fiber width, fines, and fiber freeness, and no correlation with surface properties. Vector analysis on the matrix diagram concluded that shorter fiber length, thinner fiber width, and lower fine content resulted in better two-dimensional absorbency. Additionally, a higher freeness value, indicating a lower degree of fiber refining, correlated with better two-dimensional absorbency. This is because increased fibrillation due to beating enhances hydrogen bonding between water and fibers, hindering water flow (Hossein 2022). Thus, the fiber characteristics used in manufacturing paper towels are the main factors influencing two-dimensional absorbency.

Correlation Analysis of Absorbency Analysis Factors

Based on the PCA results, a correlation analysis was performed to further investigate the factors influencing absorbency. Tables 6 and 7 present the correlation analysis results for three-dimensional and two-dimensional absorbency factors, respectively.

Table 6. Correlation Coefficient Matrix Obtained through Correlation Analysis of Three-Dimension Absorbency Analysis Factors

r Value	3D Absorbency	Porosity	Density	Freeness	*RMAD*	*FMAD*
3D absorbency	1.00					
Porosity	0.93	1.00				
Density	−0.93	−1.00	1.00			
Freeness	−0.35	−0.53	0.53	1.00		
RMAD	−0.81	−0.80	0.80	0.00	1.00	
FMAD	−0.40	−0.47	0.47	−0.06	0.71	1.00

The correlation analysis for three-dimensional absorbency (Table 6) corroborates the PCA results, showing strong correlations with porosity (r=0.93), and density (r=−0.93). In addition, the low correlations with freeness and surface properties reaffirm their limited influence on three-dimensional absorbency.

For two-dimensional absorbency (Table 7), the strongest influences were fiber length (r=−0.89) and fiber width (r=−0.85), with no significant influence from surface properties.

Table 7. Correlation Coefficient Matrix Obtained through Correlation Analysis of Two-Dimension Absorbency Analysis Factors

r Value	2D Absorbency	Fiber Length	Fiber Width	Fines	Freeness	*RMAD*	*FMAD*
2D absorbency	1.00						
Fiber length	−0.89	1.00					
Finer width	−0.85	0.90	1.00				
Fines	−0.53	0.65	0.80	1.00			
Freeness	0.62	−0.76	−0.63	−0.68	1.00		
RMAD	0.42	−0.51	−0.46	−0.35	0.00	1.00	
FMAD	−0.24	0.24	−0.50	−0.61	−0.06	0.71	1.00

CONCLUSIONS

1. This study examined both three-dimensional (3D) and two-dimensional (2D) absorbency mechanisms in paper towels. Through principal component analysis (PCA) and experimental data, key factors influencing each absorption mechanism were identified, providing a clear distinction between the roles of density structure and surface properties.
2. The tests showed that 3D absorbency is directly proportional to porosity, with strong correlation to capillary action, while 2D absorbency displayed an inverse relationship with porosity. This suggests that fluid absorption dynamics in the bulk material (3D) differ significantly from surface absorption (2D), driven by distinct physical properties.
3. Principal component analysis (PCA) identified porosity and density as the main drivers of 3D absorbency, whereas fiber length, width, fines, and freeness predominantly influenced 2D absorbency. These findings emphasize the importance of optimizing both fiber characteristics and density properties to enhance overall absorbency performance in paper products.

ACKNOWLEDGMENTS

This work was supported by the Ministry of Culture, Sports and Tourism of the Republic of Korea and the National Research Foundation of Korea (NRF) grant funded by the Korean government (NRF-2022M3C1C5A02094347).

REFERENCES CITED

Abedsoltan, H. (2022). "Wetting of paper towels: A method to determine the two-dimensional absorption capacity," *Chem. Eng. Technol.* 45(11), 2096-2102. DOI: 10.1002/ceat.202200226

Beuther, P. D., Veith, M. W., and Zwick, K. J. (2010). "Characterization of absorbent flow rate in towel and tissue," *Journal of Engineered Fibers and Fabrics* 5(2). DOI: 10.1177/155892501000500201

Brodin, F. W., and Theliander, H. (2012). "Absorbent materials based on Kraft pulp: Preparation and material characterization," *BioResources* 7(2), 1666-1683. DOI: 10.15376/biores.7.2.1666-1683

de Assis, T., Reisinger, L. W., Pal, L., Pawlak, J., Jameel, H., and Gonzalez, R. W.

(2018). "Understanding the effect of machine technology and cellulosic fibers on tissue properties – A review," *BioResources* 13(2), 4593-4629. DOI: 10.15376/biores.13.2.deassis

Hansen, E. (2013). in: *The Global Forest Sector Changes, Practices, and Prospects*, E. Hansen, R. Panwar, and R. Vlosky (eds.), CRC Press, Boca Raton, FL, USA, pp. 99-128.

Henriksson, M., Berglund, L. A., Isaksson, P., Lindström, T., and Nishino, T. (2008). "Cellulose nanopaper structures of high toughness," *Biomacromolecules* 9, 1579-1585. DOI: 10.1021/bm800038n

Hodgson, K. T., and Berg, J. C. (2007). "Dynamic wettability properties of single wood pulp fibers and their relationship to absorbency," *Wood Fiber Sci.* 20(1), 3-17.

ISO 12625-18 (2022). "Tissue paper and tissue products - Part 18: Determination of surface friction," International Organization for Standardization, Geneva.

ISO 12625-8 (2023). "Tissue paper and tissue products – Part 8: Water-absorption time and water-absorption capacity, basket-immersion test method," International Organization for Standardization, Geneva.

ISO 16065-2 (2014). "Pulps – Determination of fibre length by automated optical analysis - Part 2: Unpolarized light method," International Organization for Standardization, Geneva.

ISO 5263-1 (2004). "Pulps – Laboratory wet disintegration - Part 1: Disintegration of chemical pulps," International Organization for Standardization, Geneva.

ISO 5267-2 (2001). "Pulps – Determination of drainability - Part 2: 'Canadian Standard' freeness method," International Organization for Standardization, Geneva.

Ko, Y. C. (1981). *The Characterization and the Utilization of the Pores within the Cellulose Fibers*, Doctoral Dissertation, University of Washington.

Ko, Y. C., Lee, J. H., Kim, H. J., and Sung, Y. K. (2016). "The fundamental absorbency mechanisms of hygiene paper," *J. Korea TAPPI* 48(5), 85-97. DOI: 10.7584/jktappi.2016.10.48.5.85

Ko, Y. C., Melani, L., Park, N. Y., and Kim, H. J. (2020). "Surface characterization of paper and paperboard using a stylus contact method," *Nordic Pulp Paper Res. J.* 35(1), 78-88. DOI: 10.1515/npprj-2019-0005

Ko, Y. C., Park, J. Y., and Kim, H. J. (2017). "Characterization of surface properties of paper towels," *J. Korea TAPPI* 49(6), 81-89. DOI: 10.7584/JKTAPPI.2017.12.49.6.81

Ko, Y. C., Park, J. Y., Melani, L., Park, N. Y., and Kim, H. J. (2019). "Principles of developing physical test methods for disposable consumer products," *Nordic Pulp Paper Res. J.* 34(1), 75-87. DOI: 10.1515/npprj-2018-0029

Kweon, S. W., Ko, Y. C., Lee, Y. J., Cha, J. E., Moon, B. G., and Kim, H. J. (2024). "Determination of in-use properties of paper towels" *BioResources* 19(4), 7366-7380. DOI: 10.15376/biores.19.4.7366-7380

Kweon, S. W., Lee, Y. J., Kang, N. Y., Lee, A. Y., and Kim, H. J. (2023). "Identification of mulberry bast fiber using a multivariate analysis technique," *J. Korea TAPPI* 55(6), 59-69. DOI: 10.7584/JKTAPPI.2023.12.55.6.59

Kweon, S. W., Lee, Y. J., Lee, D. Y., Choi, J. R., and Kim, H. J. (2024). "The characteristics of wet-laid nonwoven sheet using Lyocell/wood pulp fibers," *J. Korea TAPPI* 56(2), 30-40. DOI: 10.7584/JKTAPPI.2024.4.56.2.30

Lee, J. M., Ko, Y. C., Moon, B. G., Lee, Y. J., Kweon, S. W., and Kim, H. J. (2023). "Developing physical softness models for facial tissue products," *BioResources* 19(1), 116-133. DOI: 10.15376/biores.19.1.116-133

Lee, Y. J., Ko, Y. C., Moon, B. G., and Kim, H. J. (2023). "Surface characterization

of paper products by profilometry with a fractal dimension analysis," *BioResources* 18(2), 3978-3994. DOI: 10.15376/biores.18.2.3978-3994

Moon, B. G. (2021). *Analysis of Surface Structure Characteristics of Cellulose-based Materials using Profilometry*, Doctoral Dissertation, Kookmin University, Korea.

Park, J. Y. (2017). *Effects of Pulp Fibers and Chemical Additives on Softness Component of Hygiene Paper*, Doctoral Dissertation, Kookmin University, Korea.

Park, J. Y., Melani, L., Lee, H. G., and Kim, H. J. (2020). "Effect of pulp fibers on the surface softness component of hygiene paper," *Holzforschung* 74(5), 497-504. DOI: 10.1515/hf-2019-0080

Park, N. Y., Ko, Y. C., Kim, H. J., and Moon, B. G. (2021). "Surface characterization of paper products via a stylus-type contact method," *BioResources* 16(3), 5667-5678. DOI: 10.15376/biores.16.3.5667-5678

Tanpichai, S., Sampson, W. W., and Eichhorn, S. J. (2012). "Stress-transfer in microfibrillated cellulose reinforced poly(lactic acid) composites using Raman spectroscopy," *Composites: Part A* 43, 1145-1152. DOI: 10.1016/j.compositesa.2012.02.006

Tanpichai, S., Witayakran, S., Srimarut, Y., Woraprayote, W., and Malila, Y. (2019). "Porosity, density and mechanical properties of the paper of steam exploded bamboo microfibers controlled by nanofibrillated cellulose," *Journal of Materials Research and Technology* 8(4), 3612-3622. DOI: 10.1016/j.jmrt.2019.05.024

Article submitted: July 26, 2024; Peer review completed: September 7, 2024; Revised version received and accepted: November 10, 2024: Published: November 21, 2024.
DOI: 10.15376/biores.20.1.683-697